Immunoadsorption Model for a Novel Fluidized-Bed Blood Detoxification Device

Eric A. Grovender, Charles L. Cooney, and Robert Langer
Dept. of Chemical Engineering, Massachusetts Institute of Technology, Cambridge, MA 02139

Guillermo A. Ameer
Biomedical Engineering Dept., Northwestern University, Evanston, IL 60208

A multicompartment Taylor-Couette flow hemofilter was designed to remove toxins from a patient's bloodstream via immunoadsorption. This device (Vortex Flow Plasmapheretic Reactor, VFPR) treats blood plasma with a fluidized-bed of small ($45-165\times10^{-6}$ m diameter) particles, while protecting fragile blood cells from lysis. The potential application for the VFPR is dialysis-related amyloidosis, a disease associated with the systemic accumulation of beta-2-microglobulin in patients with long-term kidney failure. The equilibrium behavior of immunoadsorptive gel beads is characterized experimentally and theoretically using confocal microscopy and the Langmuir adsorption isotherm. The importance of external mass-transfer resistance within the active compartment is assessed through dissolution studies conducted with benzoic acid particles. These results are combined with mass-transfer fundamentals to develop a dynamic immunoadsorption model. The modeling results, without the use of adjustable parameters, agree with the experimental data and provide a foundation for further development and eventual application.

Introduction

Numerous diseases are linked to elevated concentrations of soluble compounds in blood for which no adequate treatment exists because of the inability to remove them efficiently from the patient (Braun and Bosch, 2000; Schwedler et al., 2001; Tukey and Strassburg, 2000). One such condition is dialysis-related amyloidosis (DRA), a frequent complication of long-term kidney failure (Dreuke, 2000). The characteristic amyloid deposits of DRA are attributed to the systemic accumulation of β_2-microglobulin (β_2m, 1.18×10^4 g/mol), a constitutively expressed soluble protein normally cleared by healthy kidneys. Presently, there are no widely available treatments to prevent this chronic and debilitating disease, short of a kidney transplant. Conventional renal replacement technologies such as hemodialysis, hemodiafiltration, and peritoneal dialysis are believed to remove insufficient quantities of β_2m, as they are nonspecific and based on size-exclusion (Ameer, 2001).

We hypothesize that an immunoadsorptive Vortex Flow Plasmapheretic Reactor (VFPR) can be developed to remove undesired molecules from the body and thereby treat diseases such as DRA (Ameer et al., 2000). The VFPR is the first device designed to use Taylor vortex flow and particle fluidization to perform a reaction or an adsorption process on whole blood during extracorporeal therapy (Figure 1). This bioreactor was originally developed to inactivate heparin in blood through enzymatic degradation (Ameer et al., 1999b), and has more recently been used to remove β_2m from whole human blood through immunoadsorption *in vitro* (Ameer et al., 2001b).

From an engineering perspective, it would be useful to have a dynamic immunoadsorption model for the VFPR to aid in the design of device prototypes, *in vitro* experiments, and clinical trials. To derive such a model, the mass-transfer and adsorption processes within the VFPR need to be described. Towards this end, experimental and mathematical methods for characterizing the macroscopic mixing pattern within an immunoadsorptive VFPR have recently been reported

Correspondence concerning this article should be addressed to G. A. Ameer.

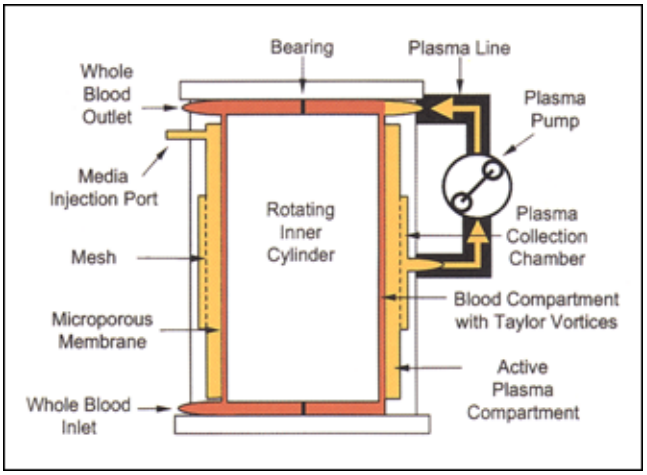

Figure 1. Vortex flow plasmapheretic reactor.

Used with permission from *Kidney International*, **59**, pp. 1544–1550 (2001). The volume of the device containing whole blood is shown in red, while the volume accessible only to plasma is shown in yellow. The prototype device had an inner cylinder radius of 2.70 cm, a membrane radius of 2.87 cm, and a membrane length of 11 cm.

(Grovender et al., 2001). Herein, the equilibrium behavior of immunoadsorptive gel beads is characterized using the Langmuir adsorption isotherm and confocal microscopy. Furthermore, the importance of external mass-transfer resistances within the active plasma compartment is assessed through dissolution studies conducted with benzoic acid particles. These results are used to develop a dynamic immunoadsorption model that should be able to describe the performance of the immunoadsorptive VFPR without using any adjustable parameters.

Description of the VFPR Device

A VFPR is constructed by counter-boring two concentric chambers within the outer cylinder wall of a Taylor-Couette vortex flow device (Ameer et al., 1999b; Figure 1). The collection chamber is sealed with a polyester mesh filter (15 μm opening) to keep the gel beads (45–165 μm diameter) within the active plasma chamber. These gel beads are highly porous and have the active species (that is, an antibody or enzyme) immobilized onto them. The active plasma compartment is sealed with a 1 μm pore-size, track-etched polyester membrane to prevent contact between blood cells and the gel beads. Compartmentalization in this novel Taylor-Couette flow device eliminates red cell lysis due to particle fluidization and prevents white cell and platelet activation due to contact with the active gel beads (Ameer et al., 1999a).

Whole blood is pumped into the inlet port (typically 200–400 mL/min) and channeled through the innermost annular or "blood" compartment. A peristaltic pump controls the plasma flow rate through the microporous membrane, the active plasma compartment, and the plasma collection chamber (typically 50–60 mL/min). The rotation of the solid inner cylinder (usually at about 1.3×10^2 rad/s) is achieved via magnetic coupling and serves to create the Taylor vortices (Donnelly, 1991) in the blood compartment. These flow instabilities induce undulations throughout the unsupported microporous membrane, fluidizing the gel beads in the active plasma compartment. The cleansed plasma exits the active plasma chamber via the collection chamber, which retains the gel beads. The cleansed plasma is returned to the top of the device where it mixes with bypassed cells and plasma prior to exiting the VFPR via the blood outlet port.

Immunoadsorptive Gel

To date, the immunoadsorptive media used with VFPR devices has consisted of anti-β_2m monoclonal antibodies immobilized onto 4% agarose gel beads (Sepharose CL-4B, Amersham-Pharmacia, Uppsala, Sweden; Ameer et al., 2001). In this section, the partitioning, diffusion, and adsorption of β_2m within the immunoadsorptive gel beads is described. These characteristics of the immunoadsorbent are used later in the derivation and solution of the dynamic immunoadsorption model equations for the VFPR.

Solute partitioning

The partition coefficient of β_2m in the gel (Φ) is defined on a total bead volume basis by Eq 1. The value of this parameter is estimated using Eq. 2 , a relation derived by Ogston (1958) for dilute solutions of uncharged, spherical macromolecules in an array of randomly arranged cylindrical fibers.

$$\Phi \equiv \frac{C_{\text{gel}}}{C_{\text{bulk}}} \tag{1}$$

$$\Phi = \exp\left[-\phi\left(1+\frac{r_s}{r_f}\right)^2\right] \tag{2}$$

Here, C_{bulk} is the concentration of desorbed β_2m in the bulk fluid, C_{gel} is the concentration of desorbed β_2m inside the beads on a total gel volume basis, and ϕ is the volume fraction of polymer fibers within the gel beads ($\phi = 0.04$). The average radius of the agarose fibers r_f was measured by small-angle X-ray scattering (Djabourov et al., 1989; $r_f = 1.9\times10^{-9}$ m). The hydrated radius of β^2m, r_s, was estimated assuming that β_2m has the specific volume and degree of hydration of a typical globular protein (Cantor and Schimmel, 1980; $r_s = 1.7\times10^{-9}$ m).

Adsorption isotherm

The antigen-antibody equilibrium dissociation constant K_D is defined by Eq. 3, while an adsorption site mass-balance is given by Eq. 4. The combination of Eqs. 1, 3, and 4 results in the Langmuir adsorption isotherm, Eq. 5

$$K_D \equiv \frac{\rho_s^{\text{eq}} C_{\text{gel}}^{\text{eq}}}{\rho_{\beta_2 m}^{\text{eq}}} \tag{3}$$

$$\rho_s^0 = \rho_s^{\text{eq}} + \rho_{\beta_2 m}^{\text{eq}} \tag{4}$$

$$\rho_{\beta_2 m}^{\text{eq}} = \frac{\rho_s^0 C_{\text{bulk}}^{\text{eq}}}{\frac{K_D}{\Phi} + C_{\text{bulk}}^{\text{eq}}} = \frac{\rho_s^0 C_{\text{gel}}^{\text{eq}}}{K_D + C_{\text{gel}}^{\text{eq}}} \tag{5}$$

On a total gel volume basis, ρ_s and $\rho_{\beta_2 m}$ are the densities of adsorption sites and adsorbed β_2m, respectively. The superscripts ^{0} and ^{eq} refer to the initial and equilibrium values, respectively.

A β_2m mass-balance (Eq. 6) can be used with Eqs. 1 and 5 to obtain Eq. 7, a form of the Langmuir adsorption isotherm in terms of measurable variables.

$$(1-\epsilon)V_{\text{bed}}\,\rho^{\text{eq}}_{\beta_2 m} = \left[V_{\text{total}} - (1-\epsilon)V_{\text{bed}}\right]\left[C^0_{\text{bulk}} - C^{\text{eq}}_{\text{bulk}}\right] + \left[(1-\epsilon)V_{\text{bed}}\right]\left[C^0_{\text{gel}} - C^{\text{eq}}_{\text{gel}}\right] \quad (6)$$

$$\left[\frac{V_{\text{total}} - V_{\text{bed}}(1-\epsilon)(1-\Phi)}{V_{\text{bed}}}\right]\left(C^0_{\text{bulk}} - C^{\text{eq}}_{\text{bulk}}\right) = \frac{(1-\epsilon)\,\rho^0_s C^{\text{eq}}_{\text{bulk}}}{\frac{K_D}{\Phi} + C^{\text{eq}}_{\text{bulk}}} \quad (7)$$

Here V_{total} is the total volume of the system, V_{bed} is the settled-bed volume of immunoadsorbent, and ϵ is the settled-bed void fraction. For cases when $\Phi \sim 1$ or $V_{\text{bed}} \ll V_{\text{total}}$, the lefthand side of Eq. 7 can be approximated as in Eq. 8

$$\left[\frac{V_{\text{total}} - V_{\text{bed}}(1-\epsilon)(1-\Phi)}{V_{\text{bed}}}\right]\left(C^0_{\text{bulk}} - C^{\text{eq}}_{\text{bulk}}\right) \approx \left[\frac{V_{\text{total}}}{V_{\text{bed}}}\right]\left(C^0_{\text{bulk}} - C^{\text{eq}}_{\text{bulk}}\right) \quad (8)$$

For the values of the parameters considered herein, this approximation represents an error of less than 2%. The adsorption site density (ρ^0_s) of the immunoadsorptive gel has previously been determined by equilibrating samples with saturating amounts of β_2m (Ameer et al., 2001). The same protocol and batch of immunoadsorbent was used with three subsaturating quantities of β_2m to produce additional data, from which the value of K_D was regressed by minimizing sum squared error (SSE).

Adsorption site distribution

Confocal microscopy was used to assess the spatial distribution of β_2m-adsorption sites within the immunoadsorbent gel beads. Recombinant human β_2m was prepared using the previously described protocol (Ameer et al., 2001) and labeled with fluorescein-5-EX succinimidyl ester, according to the instructions provided by the manufacturer (Molecular Probes, Eugene, OR). Fluorescein-β_2m (6 mg) was equilibrated with a sample of the immunoadsorptive gel (0.20 mL) in phosphate buffered saline (pH 7.4; PBS). The sample was combined with an equal volume of anti-bleaching buffer (10 μg *p*-phenylene diamine, 1.5 mL deionized water, and 1 mL 10x PBS brought to a total volume of 10 mL with glycerol) and studied with a Zeiss LSM 510 confocal microscope (Oberkochen, Germany). Two additional samples were analyzed as controls: (1) gel beads without immobilized antibody, but equilibrated with fluorescein-β_2m; (2) gel beads with immobilized antibody, but not equilibrated with fluorescein-β_2m.

Effective diffusivity

The effective diffusivity (D_e) of β_2m inside the gel beads was calculated using Eq. 9, where D_w is the diffusion coefficient of β_2m in a dilute aqueous solution and θ is the diffusion hindrance exerted by the gel polymer fibers

$$D_e = \theta D_w \quad (9)$$

The value of D_w was estimated at 37°C (1.8×10^{-10} m^2/s) using a correlation for large molecules including proteins (Polson, 1950) and θ was assumed to be the measured value (0.63) reported by Johnson et al. (1996) for lactalbumin (a 1.4×10^4 g/mol globular protein) in 4% agarose gel.

Device Model

Blood compartment

Figure 2 illustrates the dynamic adsorption model for the VFPR. It has previously been shown through residence time distribution studies and mathematical modeling that the macroscopic mixing behavior within the blood compartment can be well represented by a series of N_{BC} ideally well-mixed tanks. The residence time ($\tau_{BC,i}$) of blood plasma in each tank is constant, but each tank has its own unique volume ($V_{BC,i}$) (Grovender et al., 2001). Equations 10–14 represent a mass balance of β_2m within the blood compartment, taking into account hemofiltration into the active plasma compartment (APC)

$$\frac{dC_{BC,i}}{dt} = \frac{1}{\tau_{BC,i}}\left(C_{BC,i-1} - C_{BC,i}\right) \quad (10)$$

$$\tau_{BC,i} = \frac{(1-H_{BC,i})V_{BC,i}}{Q_{m,i} + Q_{BC,i}(1-H_{BC,i})} \quad (11)$$

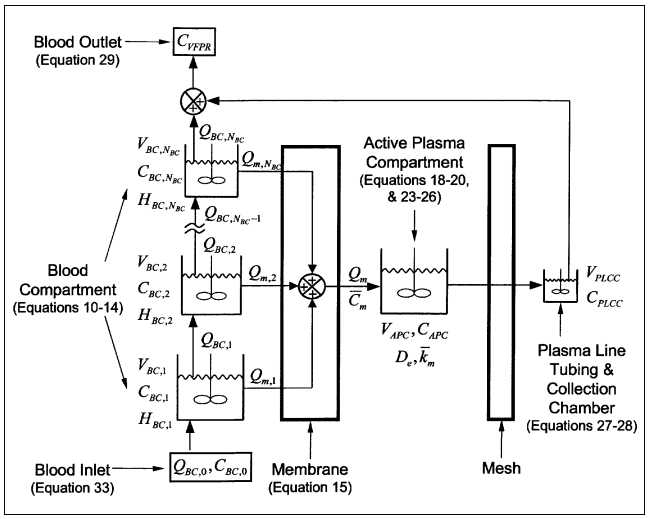

Figure 2. Dynamic VFPR adsorption model.

The macroscopic mixing behavior of the blood compartment is described by a finite series of ideally well-mixed control volumes or "tanks." The bulk fluid of the active plasma chamber and the lumped volume of the plasma line tubing and plasma collection chamber are each represented by a single tank.

$$H_{BC,i} = \frac{Q_{BC,0} H_{BC,0}}{Q_{BC,0} - \sum_{j=1}^{i} Q_{m,i}} \tag{12}$$

$$Q_{m,i} = V_{BC,i}\left(\frac{Q_m}{V_{BC}}\right) \tag{13}$$

$$Q_{BC,i} = Q_{BC,i-1} - Q_{m,i} \tag{14}$$

Here, $C_{BC,0}$, $H_{BC,0}$ and $Q_{BC,0}$ are the inlet plasma β_2m concentration, hematocrit (volume fraction of blood cells), and whole blood volumetric flow rate, respectively. The plasma pump controls the total volumetric flow rate of plasma across the microporous membrane into the active compartment Q_m. For the ith tank-in-series, $C_{BC,i}$ is the plasma concentration of β_2m, $H_{BC,i}$ is the hematocrit, $Q_{BC,i}$ is the outlet volumetric flow rate of whole blood, and $Q_{m,i}$ is the volumetric flow rate of plasma across the membrane. The total volume of the blood compartment is V_{BC}. The β_2m concentration of plasma crossing the membrane $\overline{C}_m$ is given by Eq. 15

$$\overline{C}_m = \frac{1}{V_{BC}} \sum_{i=1}^{N_{BC}} (V_{BC,i} C_{BC,i}) \tag{15}$$

Active plasma compartment

The active plasma compartment houses the immunoadsorptive media, which consists of an antibody immobilized onto porous agarose gel beads. The model for the active plasma compartment incorporates the following assumptions: (1) the intrinsic antibody-antigen association rate is instantaneous; (2) the adsorption sites are uniformly distributed inside the gel beads; (3) the adsorption equilibrium follows the Langmuir isotherm; (4) the bulk fluid within the active compartment behaves as a single well-mixed control volume as previously described (Grovender et al., 2001); (5) the size of the gel beads can be well represented by the volume-average radius R.

Equation 16 represents a mass balance for β_2m in the bulk fluid of the active plasma compartment. The first term on the righthand side of Eq. 16 accounts for convective flow through the active plasma compartment; the second term accounts for transport of β_2m to the surface of the active beads

$$\left[V_{APC} - V_{\text{bed}}(1-\epsilon)\right]\frac{dC_{APC}}{dt} = Q_m\left(\overline{C}_m - C_{APC}\right) + A_{\text{surface}}\overline{k}_m\left(C_{APC}^{\text{surface}} - C_{APC}\right) \tag{16}$$

Here V_{APC} is the total volume of the active plasma compartment and $\overline{k}_m$ is the mass-transfer coefficient for the transport of β_2m from the bulk fluid to the surface of the gel beads. The β_2m concentrations within the bulk fluid and at the outer surface of the gel beads are C_{APC} and C_{APC}^{surface}, respectively. The total surface area of the gel, A_{surface}, is expressed by Eq. 17 in terms of previously defined parameters, where N_{beads} is the total number of gel beads in the active plasma compartment

$$A_{\text{surface}} = N_{\text{beads}}(4\pi R^2) = \left[\frac{(1-\epsilon)V_{\text{bed}}}{(4\pi R^3/3)}\right](4\pi R^2) = \frac{3(1-\epsilon)V_{\text{bed}}}{R} \tag{17}$$

Equations 1, 16, and 17 are combined to yield Eq. 18, which, along with Eqs. 19 and 20, are used to model the dynamics of the β_2m concentration of the bulk fluid within the active plasma compartment

$$\frac{dC_{APC}}{dt} = \frac{1}{\tau_{APC}}\left(\overline{C}_m - C_{APC}\right) + \frac{3V_{\text{bed}}(1-\epsilon)}{\tau_{EMT}\left[V_{APC} - V_{\text{bed}}(1-\epsilon)\right]}\left(\frac{C_{\text{gel}}^{\text{surface}}}{\Phi} - C_{APC}\right) \tag{18}$$

$$\tau_{APC} = \frac{V_{APC} - V_{\text{bed}}(1-\epsilon)}{Q_m} \tag{19}$$

$$\tau_{EMT} = \frac{R}{\overline{k}_m} \tag{20}$$

Here, the characteristic time-scale of external mass transfer (or the transport of β_2m to the surface of the active beads) is τ_{EMT} and τ_{APC} is the residence time of the bulk fluid volume.

Using the aforementioned assumptions, the species conservation equation for desorbed β_2m within an immunoadsorptive gel bead is reduced to the form shown by Eq. 21. The rate of adsorption $R_{\text{adsorption}}$ is expressed in the convenient form shown by Eq. 22

$$\frac{\partial C_{\text{gel}}}{\partial t} = D_e \frac{1}{r^2}\frac{\partial}{\partial r}\left(r^2 \frac{\partial C_{\text{gel}}}{\partial r}\right) - R_{\text{adsorption}} \tag{21}$$

$$R_{\text{adsorption}} = \frac{\partial \rho_{\beta_2 m}}{\partial C_{\text{gel}}}\left(\frac{\partial C_{\text{gel}}}{\partial t}\right) \tag{22}$$

The Langmuir adsorption isotherm, or Eq. 5, is combined with Eqs. 21 and 22 to yield Eqs. 23 and 24 which represent a mass balance for β_2m within a gel bead. Here, the characteristic time-scale of internal mass transfer within the porous beads is τ_{IMT}. Equation 23 has previously been derived and used to model the adsorption of albumin onto an ion-exchange resin (Leaver et al., 1992). Equations 25 and 26 represent the boundary conditions that were used to solve Eq. 23, where the superscripts $^{\text{surface}}$ and $^{\text{center}}$ refer to their respective radial positions

$$\frac{\partial C_{\text{gel}}}{\partial t} = \frac{R^2}{\tau_{IMT}}\left(1 + \frac{\rho_S^0 K_D}{\left(K_D + C_{\text{gel}}\right)^2}\right)^{-1}\left(\frac{\partial^2 C_{\text{gel}}}{\partial r^2} + \frac{2}{r}\frac{\partial C_{\text{gel}}}{\partial r}\right) \tag{23}$$

$$\tau_{IMT} = \frac{R^2}{D_e} \tag{24}$$

$$\bar{k}_m\left(C_{APC}-\frac{C_{\text{gel}}^{\text{surface}}}{\Phi}\right)=D_e\left(\frac{\partial C_{\text{gel}}}{\partial r}\right)^{\text{surface}} \tag{25}$$

$$\left(\frac{\partial C_{\text{gel}}}{\partial r}\right)^{\text{center}}=0 \tag{26}$$

Plasma line, collection chamber, and blood outlet port

The plasma line and collection chamber are lumped together as a single well-mixed control volume and modeled by Eqs. 27–28. Here C_{PLCC}, V_{PLCC}, and τ_{PLCC} are the lumped β_2m concentration, volume, and residence time, respectively. The plasma β_2m concentration of partially cleansed whole blood exiting the VFPR, C_{VFPR}, is calculated by Eq. 29

$$\frac{dC_{PLCC}}{dt}=\frac{1}{\tau_{PLCC}}(C_{APC}-C_{PLCC}) \tag{27}$$

$$\tau_{PLCC}=\frac{V_{PLCC}}{Q_m} \tag{28}$$

$$C_{VFPR}=\frac{Q_mC_{PLCC}+(Q_{BC,0}-Q_m)(1-H_{BC,N_{BC}})C_{BC,N_{BC}}}{Q_{BC,0}(1-H_{BC,0})} \tag{29}$$

Reservoir Model

The VFPR is usually connected to a β_2m reservoir in a closed-loop circuit for blood detoxification (Figure 3). This reservoir can be comprised of a bag of donated blood, an animal model, or a human patient. To date, β_2m-immunoadsorption experiments with the VFPR have been limited to bags of whole human blood (Ameer et al., 2001). Equations 30 and 31 represent the mass balance of β_2m in a blood bag (530 mL) and its circuit tubing (65 mL). These two volumes are lumped together as V_{BR}. Equations 32 and 33 mathematically connect the reservoir to the VFPR device in a closed-loop circuit

$$\frac{dC_{BR,i}}{dt}=\frac{1}{\tau_{BR,i}}(C_{BR,i-1}-C_{BR,i}) \tag{30}$$

$$\tau_{BR,i}=\frac{\tau_{BR}}{N_{BR}}=\frac{V_{BR}}{N_{BR}Q_{BR}} \tag{31}$$

$$C_{BR,0}=C_{VFPR} \tag{32}$$

$$C_{BC,0}=C_{BR,N_{BR}} \tag{33}$$

Here, N_{BR} is the number of theoretical tanks representing V_{BR}. For the ith tank-in-series, $C_{BR,i}$ is the plasma β_2m concentration and $\tau_{BR,i}$ is the residence time.

Characterization of Mass-Transfer to the Surface of Suspended Particles

The importance of mass-transfer resistance at the external surface of the suspended gel beads (τ_{EMT}, Eq. 20) relative to the mass-transfer resistance associated with the hemofiltration rate (τ_{APC}, Eq. 19) was assessed through dissolution studies conducted with small, nonspherical particles of benzoic acid. These particles were created using a method similar to one previously described by Moore (1994). Briefly, benzoic acid was melted, solidified into a flat sheet on aluminum foil, and crushed with a ceramic mortar and pestle. Irregularly shaped particles approximately 100 μm in size were obtained by sifting the crushed benzoic acid between 150 μm and 75 μm nominal opening stainless steel sieves (VWR, Westchester, PA).

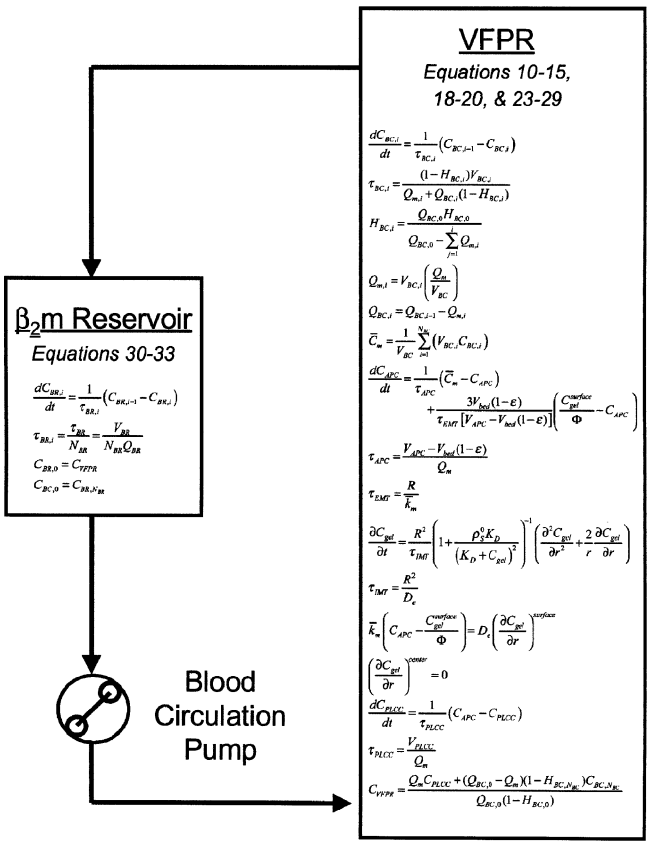

Figure 3. Closed-loop blood detoxification with the VFPR.

The β_2m reservoir represents either a human patient or a substituted model (that is, a bag of blood) and the circuit tubing. The equations shown are provided as a convenience to the reader and are described throughout the text.

The dissolution studies were conducted as shown in Figure 4. The active plasma compartment was flushed for 5 min (>3.5 residence times) to remove most ($>95\%$) of the dissolved benzoic acid that was injected along with the solid particles. During the following 5 min experimental period, samples were taken every 60 s and immediately filtered to remove any remaining fine particles (0.45 μm Millipore catalog number SLHV R04 NL, Bedford, MA). The concentration of benzoic acid was measured by reading the absorbance at 250×10^{-9} m (diluting the samples as necessary with 0.01% Triton X-100).

Computational Methods

Equations 10–15, 18–20, and 23–33 model the dynamics of β_2m adsorption within the VFPR and the subsequent removal of β_2m from a blood reservoir. The forward-time centered-space (FTCS) method was used to convert Eq. 23 into a discrete form (200 finite radial sections), and the second-order

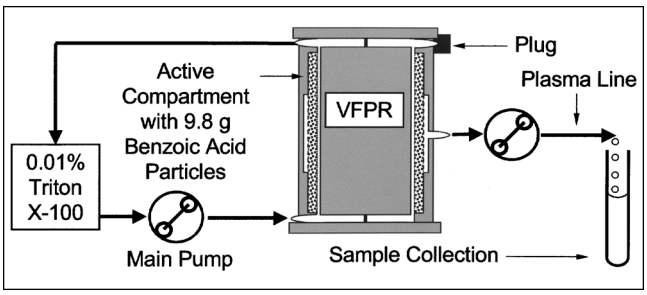

Figure 4. Apparatus used to conduct the dissolution studies.

Agarose gel beads (40 mL Sepharose CL-4B) were included in the active compartment in an attempt to duplicate the conditions of the dynamic β_2m-adsorption experiments. The main pump flow rate (200 mL/min), plasma pump flow rate (50 mL/min), and cylinder rotation rate (1.3×10^2 rad/s) also matched those used during the β_2m-adsorption experiments. Aggregation of the benzoic acid particles was prevented by adding 0.01% Triton X-100 to the system. It has previously been reported that the use of a similar nonionic surfactant during benzoic acid dissolution studies has a minimal effect (< 5%) on the mass-transfer rate (Gondoh et al., 1968).

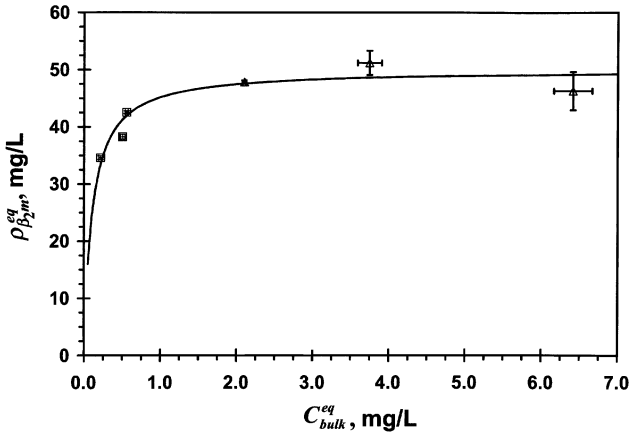

Figure 5. Equilibrium adsorption behavior of the immunoadsorptive media.

Equations 7 and 8 (—) were regressed to the saturated (Δ) (Ameer et al., 2001) and subsaturated (□) data to determine the value of K_D (0.1 ± 0.1 mg/L ~ 10^{-8} mol/L). The value of ρ_s^0 (50 ± 3 mg/L) was calculated from the saturated data. Error bars and confidence intervals represent the standard error of the mean (SEM).

Runge-Kutta algorithm was applied to integrate the differential equations (Press et al., 1992). Input parameters (including initial conditions, with superscripts $^{t=0}$) used for the model calculations are listed in Table 1. At each time-step, the total mass-balance error for Eqs. 10–15, 18–20, and 23–33 was kept below 0.5%.

Results and Discussion

We designed a multicompartment Taylor-Couette flow hemofilter to remove toxins from a patient's bloodstream via immunoadsorption. The first immunoadsorption application was to remove the amyloid-associated protein β_2-microglobulin from human blood *in vitro*. This technology, we believe, can be used for understanding and treating the progression of dialysis-related amyloidosis, a devastating complication of long-term kidney failure, by targeting a specific macromolecule and monitoring the effect of its removal on the patient via clinical trials. To lay a solid foundation for the derivation of a dynamic model, the equilibrium behavior of the immunoadsorbent and the mass-transfer characteristics of the VFPR were investigated independently.

Table 1. Model Input Parameters

Parameter	Value	Parameter	Value
$c_{APC}^{t=0}$	0 mg/L	Q_m	50* mL/min
$C_{BC,i}^{t=0}$	3.2* mg/L	R	46‖ μm
$C_{BR,i}^{t=0}$	3.2* mg/L	V_{BC}	46.5‡,§ mL
$C_{gel}^{t=0}$	0 mg/L	$V_{BC,i}$	6.6, 6.3, 6.1, 5.9 mL
$C_{PLCC}^{t=0}$	0 mg/L		5.7, 5.5, 5.3, 5.1‡,§
D_e	1.1×10^{-10} m²/s	V_{APC}	79‡ mL
H_{BR}	0.31*,†	V_{bed}	48* mL
K_D	0.1 mg/L	V_{BR}	595* mL
$\bar{k}_m$	10^{-3} m/s	V_{PLCC}	15* mL
N_{BC}	8‡,§	ϵ	0.4#
N_{BR}	3‡,§	Φ	0.87
Q_{BR}	200* mL/min	ρ_s^0	50*,## mg/L

*Ameer et al., 2001.
†After accounting for dilution by the priming saline.
‡Grovender et al. (2001).
§The mixing behavior was re-characterized through similar RTD studies using a 36% glycerol-in-water solution at 20°C to better account for the viscosity and density of whole blood (Wolf et al., 1984; Fournier, 1999).
‖Data provided by the manufacturer.
#Calculated from the total and void volumes measured in a packed column (acetone and pore-excluded aggregate protein markers; Bio-Rad No. 151-1901, Hercules, CA).
##Value previously reported on a settled-bed volume basis.

Over the β_2m concentration range considered, the Langmuir isotherm describes equilibrium β_2m adsorption data (Figure 5). The value of the antibody-antigen dissociation constant ($K_D = 0.1 \pm 0.1$ mg/L) is significantly smaller than the lower limit of the β_2m concentration range in the circulation of healthy individuals (1.0–3.0 mg/L) (Floege and Ketteler, 2001). Therefore, this model immunoadsorbent appears to have sufficient affinity for therapeutic application.

The cross-sectional confocal micrograph of a typical immunoadsorptive gel bead shows that the β_2m adsorption sites are uniformly distributed throughout the polymer (Figure 6a). This was a key assumption in the numerical solution of Eq. 23 (that is, ρ_s^0 not a function of radial position). Meanwhile, the defect in the atypical bead demonstrates the ability of the imaging technique to detect regions inside the gel that lack adsorbed β_2m (Figure 6b). These results demonstrate the utility of confocal microscopy for the characterization of porous matrices.

During the dissolution studies, the observed concentration of benzoic acid (3.0 ± 0.1 g/L) exiting the VFPR through the plasma line did not significantly differ from the solubility limit (2.9 g/L at 20°C) (Budavari et al., 1989). This strongly suggests that external mass-transfer resistances within the active plasma compartment are not rate limiting under the process conditions considered. In order to provide flexibility for other process conditions that may arise in the future, the derivation of the VFPR model accounts for the possibility of a rate-

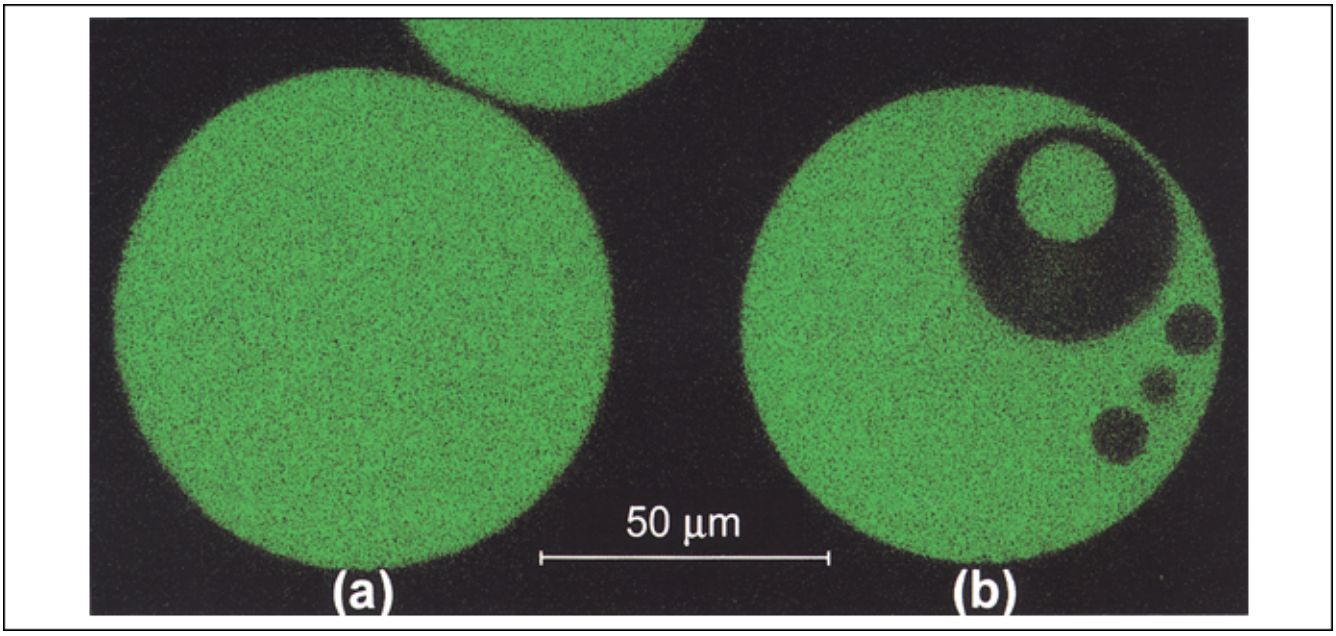

Figure 6. Confocal micrograph of the immunoadsorptive gel: center cross-section of (a) typical bead; (b) atypical bead.

β_2m is shown in green. The controls showed no apparent adsorption of β_2m or intrinsic fluorescence of the immunoadsorbent. The thickness of the cross-section shown is 0.40 μm and the resolution is 0.22 μm.

limiting external mass-transfer resistance through the mass-transfer coefficient $\bar{k}_m$. In accordance with the findings of the dissolution studies $\bar{k}_m$ was assigned a finite value sufficiently large such that $\tau_{EMT} \ll \tau_{IMT}$ and $\tau_{EMT} \ll \tau_{APC}$ (Table 1 and Eqs. 19, 20 and 24). Thus, external mass-transfer resistance did not have any appreciable effect on the immunoadsorption dynamics calculated by the model for the experiment considered (refer to the sensitivity analysis below and Figure 8a). However, the second term on the righthand side of Eq. 18 is required in any case to account for the transport of β_2m to the surface of the gel beads.

The model's ability to describe VFPR performance was tested with a set of input parameters corresponding to a previously conducted β_2m-adsorption experiment (Table 1). Without adjusting any of the parameters, the dynamic immunoadsorption model is able to describe the performance of the VFPR (Figure 7; Eqs. 10–15, 18–20 and 23–33). It is important to note that the equilibrium concentration of β_2m is on the order of the antibody-antigen dissociation constant (K_D). This is the case because the system was charged, approximately, with a 1:1 stoichiometric ratio of β_2m and adsorption sites. Under clinical operating conditions, an immunoadsorptive VFPR would likely contain an excess number of adsorption sites. In separate β_2m immunoadsorption experiments that were conducted with excess adsorption sites, the equilibrium β_2m concentrations were below detectable limits (Ameer et al., 2001).

A sensitivity analysis was conducted on the external mass-transfer coefficient ($\bar{k}_m$) to confirm that increasing the value of $\bar{k}_m$ above the arbitrarily assigned value does not have a significant effect on the model predictions (Figure 8a). Furthermore, the model's flexibility to account for external mass-transfer resistances is demonstrated by the shape of the plasma line model curve for the low value of $\bar{k}_m$ ($\tau_{EMT} \sim \tau_{IMT}$). The assumption that the population of gel beads can be well represented by the volume-average radius was tested by a sensitivity analysis on R (Figure 8b). Varying the value of this parameter by one standard of deviation has an effect on the shape of the plasma line concentration curve; however, this effect is reasonably symmetric. Therefore, the assumption appears to be justified. Because their values were

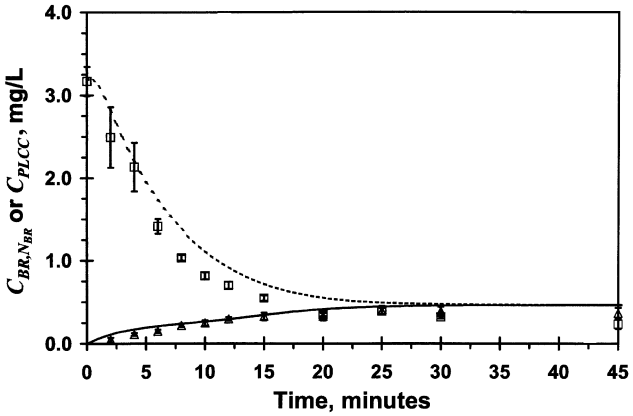

Figure 7. Predicted and observed dynamics of β_2m clearance from whole blood by an immunoadsorptive VFPR, *in vitro*.

The model equations listed in Figure 3 and the input parameters listed in Table 1 were used to calculate the blood reservoir outlet ($C_{BR,N_{BR}}$, - - - -) and plasma line (C_{PLCC}, —) β_2m concentrations. The blood reservoir outlet (□) and plasma line (△) data has been previously reported (Ameer et al., 2001). Error bars represent SEM.

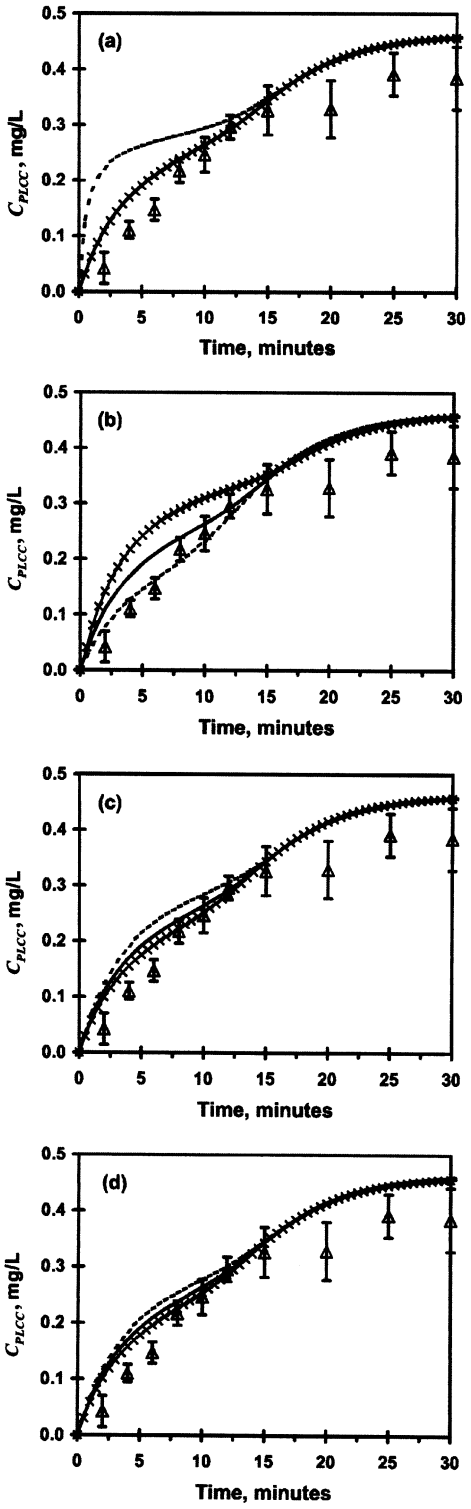

Figure 8. Figure 8. Sensitivity analysis for the model parameters (a) $\bar{k}_m$, (b) R, (c) D_e and (d) Φ.

The plasma line data (△) has previously been reported (Ameer et al., 2001) and the error bars represent the standard error of the mean (SEM). The center (—) values for the model parameters are listed in Table 1. The high (-×-×-) and low (- - - -) values are as follows: $\bar{k}_m = 10^{-2}$ and 10^{-5} m/s, $R = 58$ & 34 μm($\pm\sigma$), $D_e = 1.8\times10^{-10}$ and 0.7×10^{-10} m^2/ ($\pm$20%), $\Phi = 1.00$ & 0.75 (the measured value reported by Johnson et al. (1995) for lactalbumin in 6% agarose gel).

estimated from the literature, sensitivity analyses on the hindered effective diffusivity (D_e) and the solute partition coefficient (Φ) were performed (Figures 8c–8d). The variations considered (refer to Figure 8 caption) in D_e and Φ resulted in changes of less than 15% in the calculated values of C_{PLCC} at all time points.

The dynamic immunoadsorption model for the VFPR was developed to facilitate the development of the device and the optimization of its potential therapeutic application. With the desire for a model capable of describing the VFPR's performance over a range of conditions, the model was based on a fundamental transport theory and guided by the independent characterization of the fluid dynamics and adsorption equilibrium. The model calculations predict that the mass-transfer processes within the active compartment of the VFPR do not control the rate of β_2m-adsorption (Figure 7). Hence, we conclude that the process controlling the β_2m-adsorption rate within the VFPR is the hemofiltration rate ($Q_m = 50$ mL/min), which is on the order of the reported flow rate of extravascular β_2m into the bloodstream (~ 70 mL/min) (Floege et al., 1991). These two processes are expected to be rate-controlling for β_2m removal from a patient with the immunoadsorbent VFPR. A major goal for the future development of the VFPR will be to increase the hemofiltration rate, while maintaining the fast mass-transfer rates within the active plasma compartment. The methods for characterizing the VFPR and the dynamic immunoadsorption model presented herein should prove useful in this endeavor.

Acknowledgments

This work was supported in part by a National Institute of Health Biotechnology Training Grant and the National Kidney Foundation. Furthermore, this work was conducted utilizing the W. M. Keck Foundation Biological Imaging Facility at the Whitehead Institute. The authors would like to thank Professor W. M. Deen for his insightful discussion and Gordana Vunjak-Novakovic for her comments on the manuscript.

Literature Cited

Ameer, G. A., W. Harmon, R. Sasisekharan, C. Cooney, and R. Langer, "Investigation of a Whole Blood Fluidized Bed Taylor-Couette Flow Device for Enzymatic Heparin Neutralization," *Biotechnol. Bioeng.*, **62**, 602 (1999a).

Ameer, G. A., G. Barabino, R. Sasisekharan, W. Harmon, C. L. Cooney, and R. Langer, "*Ex Vivo* Evaluation of a Taylor-Couette Flow, Immobilized Heparinase I Device for Clinical Application," *PNAS USA*, **96**, 2350 (1999b).

Ameer, G., R. S. Langer, M. Rupnick, H. L. Ploegh, and E. Grovender, "Apparatus for Treating Whole Blood Comprising Concentric Cylinders Defining an Annulus There Between," U.S. Patent No. 6,099,730 (2000).

Ameer, G. A., "Modalities for the Removal of β_2-microglobulin from Blood," *Semin. Dialysis*, **14-2**, 103 (2001).

Ameer, G. A., E. A. Grovender, H. Ploegh, D. Ting, W. F. Owen, M. Rupnick, and R. Langer, "A Novel Immunoadsorption Device for Removing β_2-microglobulin from Whole Blood," *Kidney Int.*, **59**, 1544 (2001).

Budavari, S., M. J. O'Neil, A. Smith, and P. E. Heckelman, *The Merck Index*, 11th ed., Merck & Co., Rahway, NJ, p. 170 (1989).

Braun, N., and T. Bosch, "Immunoadsorption, Current Status and Future Developments," *Exp. Opin. Invest. Drugs*, **9**, 2017 (2000).

Cantor, C. R., and P. R. Schimmel, *Biophysical Chemistry: Techniques for the Study of Biological Structure and Function*, W. H. Freeman and Co., New York, pp. 554–555 (1980).

Djabourov, M., A. H. Clark, D. W. Rowlands, and S. B. Ross-Murphy,

"Small-Angle X-Ray Scattering Characterization of Agarose Sols and Gels," *Macromol. Rev.*, **22**, 180 (1989).
Donnelly, R. J., "Taylor-Couette Flow: The Early Days," *Phys. Today*, **44**, 32 (1991).
Drueke, T., "β_2-microglobulin and Amyloidosis," *Nephrol. Dial. Transplant.*, **15**, 17 (2000).
Floege, J., A. Bartsch, M. Schulze, S. Shaldon, K. M. Koch, and C. Smeby, "Clearance and Synthesis Rates of β_2-microglobulin in Patients Undergoing Hemodialysis and in Normal Subjects," *J. Lab. Clin. Med.*, **118**, 153 (1991).
Floege, J., and M. Ketteler, "β_2-microglobulin-Derived Amyloidosis: an Update," *Kidney Int.*, **59**, S-164-171 (2001).
Fournier, R. L., *Basic Transport Phenomena in Biomedical Engineering*, Taylor & Francis, Philadelphia, p. 65 (1999).
Grovender, E. A., C. L. Cooney, R. S. Langer, and G. A. Ameer, "Modeling the Mixing Behavior of a Novel Fluidized Extracorporeal Immunoadsorber," *Chem. Eng. Sci.*, **56**(18), 5437 (2001).
Gondoh, S., M. Shiozawa, K. Kusunoki, and I. Nakamori, "Effects of Surfactants on the Solution Rate of Single Benzoic Acid Spheres in Water," *Kagaku Kogaku*, **32**, 919 (1968).
Johnson, E. M., D. A. Berk, R. K. Jain, and W. M. Deen, "Diffusion and Partitioning of Proteins in Charged Agarose Gels," *Biophysical J.*, **68**, 1561 (1995).
Johnson, E. M., D. A. Berk, R. K. Jain, and W. M. Deen, "Hindered Diffusion in Agarose Gels: Test of the Effective Medium Model," *Biophys. J.*, **70**, 1017 (1996).
Leaver, G., J. A. Howell, and J. R. Conder, "Adsorption Kinetics of Albumin on a Cross-Linked Cellulose Chromatographic Ion Exchanger," *J. Chromatog.*, **590**, 101 (1992).
Moore, C. M. V., "Characterization of a Taylor-Couette Vortex Flow Reactor," PhD Thesis, Dept. of Chemical Engineering, MIT, Cambridge, MA, 83 (1994).
Ogston, A. G., "The Spaces in a Uniform Random Suspension of Fibers," *Trans. Faraday Soc.*, **54**, 1754 (1958).
Polson, A., "Some Aspects of Diffusion in Solution and a Definition of a Colloid Particle," *J. Phys. Colloid Chem.*, **54**, 649 (1950).
Press, W. H., S. A. Teukolsky, W. T. Vetterling, and B. P. Flannery, *Numerical Recipes in Fortran 77: The Art of Scientific Computing*, Cambridge University Press, New York, pp. 704, 838 (1992).
Schwelder, S., R. Schinzel, P. Vaith, and C. Wanner, "Inflammation and Advanced Glycation End Products in Uremia: Simple Coexistence, Potentiation or Causal Relationship?" *Kidney Int.*, **59**, S32 (2001).
Tukey, R. H., and C. P. Strassburg, "Human UDP-Glucuronosyltransferases: Metabolism, Expression, and Disease," *Annu. Rev. Pharmacol. Toxicol.*, **40**, 581 (2000).
Wolf, A. V., M. G. Brown, and P. G. Prentiss, "Concentrative Properties of Aqueous Solutions: Conversion Tables," *CRC Handbook of Chemistry and Physics*, R. C. Weast, M. J. Astle, and W. H. Beyer, eds., 65th ed., CRC Press. Boca Raton, FL, p. D-235 (1984).

Manuscript received Aug. 8, 2001, and revision received Mar. 25, 2002.